Charge transfer and fragmentation in cluster-atom collisions

O. Knospe

Max-Planck-Institut für Physik Komplexer Systeme, Nöthnitzer Strasse 38, 01187 Dresden, Germany

J. Jellinek

Chemistry Division, Argonne National Laboratory, Argonne, Illinois 60439

U. Saalmann

Atomfysik, Stockholms Universitet, Frescativägen 24, 10405 Stockholm, Sweden

R. Schmidt

Institut für Theoretische Physik, Technische Universität Dresden, 01062 Dresden, Germany

Charge transfer and fragmentation in collisions of sodium cluster ions with caesium atoms have been investigated theoretically within a microscopic framework called nonadiabatic quantum molecular dynamics. To illustrate the complexity of nonadiabatic cluster collisions, in particular the interplay between charge transfer and fragmentation, $Na_4^+(2.7 \text{ keV})+Cs$ collisions are studied in detail with special emphasis on methodical aspects. It is shown that integral and exclusive charge transfer cross sections can be understood only if all types of fragmentation processes including statistical decay are taken into account. The influence of the cluster structure (isomers, temperature, size) on measured and measurable cross sections is studied for different charge transfer channels as well as for fragmentation. In particular, cross sections for the exotic formation of caesium anions in such collisions are predicted.

PACS number(s): 34.70.+e, 36.40.Qv, 31.15.Qg

I. INTRODUCTION

Charge transfer represents one of the most frequently studied phenomena in the field of ion-atom scattering. The results of these numerous investigations (see Ref. [1] for an overview) improved our understanding of the fundamental atomic interactions and provided microscopic ''background information'' for applications in plasma physics and even astrophysics. On the other hand, considerable progress has also been achieved in the investigation of the complex ion-surface interactions [2]. In order to close the gap between these two limiting cases, charge transfer in cluster collisions have been the subject of many recent activities [3–20].

In general, the fundamental processes accompanying cluster collisions include electronic transitions (excitation, charge transfer, ionization) and energy transfer in nuclear degrees of freedom (vibrations, rotations, fragmentation). In *nonadiabatic* cluster collisions these take place simultaneously involving a moderate to large (but finite) number of electronic and nuclear degrees of freedom. In particular, the coupling of electronic and atomic degrees of freedom (electron-vibration or ''vibronic'' coupling) is of special interest. E.g., collision-induced electronic excitation can be transferred into vibrational motion resulting in fragmentation [21].

A considerable amount of experimental data on charge transfer (CT) in cluster collisions has been accumulated. In one of the first experiments with mass-selected cluster beams CT and fragmentation were investigated for $Na_n^+ + Cs$ [3,4] and $K_n^+ + Cs$ [4] collisions. Subsequent experimental studies included collisions of cluster cations with atoms [5–10], molecules [7], and clusters [9,11]. In collisions of highly charged ions with fullerenes [12,13] and sodium clusters [14]

multiple CT processes accompanied by fragmentation have been observed. Very recently, CT in collisions of sodium-cluster ions with laser-excited sodium atoms has been investigated [15].

In contrast to the rich experimental material the number of theoretical investigations on CT in cluster collisions is rather small. A two-state model of (near) resonant CT was presented in Ref. [4]. Classical barrier models [16,17] have been used to study distant collisions of C_{60} with highly charged ions. Semimicroscopic descriptions of CT have been developed with the jellium model for sodium clusters ($Na_{19}^+ + Na$ [18]) or with an ''independent-electron'' model ($H^+ + Na_n$ [19]). However, the simultaneous description of CT *and* fragmentation or, in general, of electronic *and* nuclear degrees of freedom in nonadiabatic cluster collisions requires a fully microscopic theoretical approach. The recently developed nonadiabatic quantum molecular dynamics (NA-QMD [22]) allows to cope with such situations.

Applications of the NA-QMD approach on cluster collisions [23,15,21,20] opened insight into the reaction mechanism of nonadiabatic cluster collisions and revealed interesting new phenomena. In collaboration with the experimental groups the mechanism of collision-induced dissociation has been investigated for $Na_2^+ + He$ [23]. A strong temperature dependence of CT has been found in $Na_n^+ + Na$ collisions with electronically excited target atoms [15]. A general study of excitation and relaxation in sodium-cluster collisions [21] provided insight into the mechanism of the vibronic coupling. In particular, a ''transparency window'' in the energy dependence of the fragmentation cross section for collisions of ''closed shell'' clusters was predicted. Indications for this effect have recently been found experimentally in He^+

$+C_{60}$ collisions [24]. In a preceding paper [20] CT in $Na_n^+ + Cs$ collisions has been studied. It has be shown that an understanding of the measured CT cross sections [3] can only be achieved if the complete scenario of the collision, in particular the interplay between CT and fragmentation, is properly described [20].

In this paper we present a detailed analysis of CT and fragmentation in $Na_n^+ + Cs$ collisions ($4 \leq n \leq 11$) using the NA-QMD approach. Special emphasis is put on the discussion of methodical problems. Isomer, size and temperature dependence of the cross sections are studied in detail. The theoretical framework is sketched in Sec. II, whereby the equations of motion of the NA-QMD approach are presented in Sec. II A, and the calculation of CT probabilities is described in Sec. II B. The methodical aspects, i.e., how to obtain theoretical cross sections which are directly comparable with experimental data, are discussed exemplary for $Na_4^+ (2.7 \text{ keV}) + Cs$ in Sec. III A including temperature effects. The isomer and size dependence of CT and fragmentation cross sections for $Na_n^+ (2.7 \text{ keV}) + Cs$ collisions are the subject of Sec. III B. Calculated cross sections for the ''exotic'' CT channel characterized by the formation of Cs^-, which was predicted to have a finite probability [20], are presented in Sec. III C closing with summary and outlook in Sec. IV.

II. THEORETICAL

A. Equations of motion

Within the NA-QMD approach, electronic (quantum) and atomic (classical) degrees of freedom are treated simultaneously and self-consistently by combining time-dependent density functional theory with molecular dynamics (MD).

The basic theorem of time-dependent density functional theory [25,26] states that for a system of interacting particles the many-particle state and, thus, any observable are *uniquely* determined by the time-dependent single-particle density $\rho(\mathbf{r},t)$ which can be written identically as the density of a non-interacting reference system $\rho(\mathbf{r},t) = \sum_j^{N_e} |\psi^j(\mathbf{r},t)|^2$ with N_e the number of electrons. The single-particle functions ψ^j are obtained from the time-dependent Kohn-Sham (KS) equations (all formulas are written in atomic units)

$$i\frac{\mathrm{d}}{\mathrm{d}t}\psi^j(\mathbf{r},t) = \{\hat{t} + V_{\text{eff}}(\mathbf{r},t)\}\psi^j(\mathbf{r},t), \tag{1}$$

which result from the minimization of the electronic action integral [26]. The single-particle Hamilton operator in Eq. (1) contains besides the kinetic energy operator $\hat{t}$ a *local* effective potential

$$V_{\text{eff}}(\mathbf{r},t) = V_{\text{eff}}[\rho](\mathbf{r},t)$$

$$= V(\mathbf{r},\mathbf{R}) + \int d^3r' \frac{\rho(\mathbf{r}',t)}{|\mathbf{r}-\mathbf{r}'|} + V_{\text{xc}}[\rho](\mathbf{r},t). \tag{2}$$

The capital $\mathbf{R}$ is used (here and later on) as abbreviation for the positions $\mathbf{R}_1, \ldots, \mathbf{R}_{N_n}$ of all N_n nuclei. The potential (2) consists on the one hand of an external potential $V(\mathbf{r},\mathbf{R})$, which in our case is time-dependent owing to the atomic motion $\mathbf{R}(t)$. On the other hand, there are electron-electron interaction terms, namely the Hartree and the exchange-correlation term, which depend both via the density ρ on the functions ψ^j. The actual approximation for the exchange-correlation potential V_{xc} will be specified below.

For the description of collision processes it is favorably to write the KS functions as linear combinations of atomic orbitals $\phi_\alpha(\mathbf{r} - \mathbf{R}_{A_\alpha})$ which move along the classical trajectories $\mathbf{R}_{A_\alpha}(t)$

$$\psi^j(\mathbf{r},t) = \sum_\alpha \phi_\alpha(\mathbf{r} - \mathbf{R}_{A_\alpha}) a_\alpha^j(t). \tag{3}$$

Here, A_α denotes the atom at which the function ϕ_α is centered. By inserting the LCAO ansatz (3) into the KS equations (1) one arrives at

$$\dot{a}_\alpha^j(t) = -\sum_{\beta\gamma}(S^{-1})_{\alpha\beta}\left\{iH_{\beta\gamma} + \sum_A^{N_n}\dot{\mathbf{R}}_A\mathbf{R}_{\beta\gamma}^A\right\}a_\gamma^j(t) \tag{4}$$

with the overlap matrix $S_{\alpha\beta} \equiv \langle\phi_\alpha|\phi_\beta\rangle$, the Hamilton matrix $H_{\alpha\beta} \equiv \langle\phi_\alpha|\hat{t}+V_{\text{eff}}|\phi_\beta\rangle$, and the coupling matrix $\mathbf{R}_{\alpha\beta}^A \equiv \langle\phi_\alpha|\partial\phi_\beta/\partial\mathbf{R}_A\rangle$. Note that Eq. (4) is highly nonlinear, owing to the density dependence of the effective potential V_{eff} which enters the Hamilton matrix $H_{\alpha\beta}$.

The corresponding Newton equations for the N_n nuclei can be derived by using the conservation of the total energy of the system leading to [22]

$$\begin{aligned} M_A\ddot{\mathbf{R}}_A = &-\frac{\partial\sum_B^{N_n}{}'}{\partial R_A}\frac{Z_A Z_B}{|\mathbf{R}_A-\mathbf{R}_B|} - \sum_j^{N_e}\left\{\sum_{\alpha\beta}\bar{a}_\alpha^j\left(\frac{\partial H_{\alpha\beta}}{\partial R_A}\right)a_\beta^j\right. \\ &-\sum_{\alpha\beta}\bar{a}_\alpha^j\left\langle\phi_\alpha\left|\frac{\partial(V_{\text{eff}}-V)}{\partial R_A}\right|\phi_\beta\right\rangle a_\beta^j \\ &-\sum_{\alpha\beta\gamma\delta}[\bar{a}_\alpha^j H_{\alpha\beta}(S^{-1})_{\beta\gamma}\mathbf{R}_{\gamma\delta}^A a_\delta^j \\ &\left.+\bar{a}_\alpha^j(\mathbf{R}^{\mathrm{T}})_{\alpha\beta}^A(S^{-1})_{\beta\gamma}H_{\gamma\delta}a_\delta^j]\right\}. \end{aligned} \tag{5}$$

The force on the right-hand side of Eq. (5) contains besides the collective term of the nucleus-nucleus repulsion (first line) and expectation values of gradients (second and third line) further terms (fourth and fifth line) which guarantee that the total energy of the system is conserved even for finite, local basis sets. These additional terms depend strongly on the applied basis set.

The time-dependent KS equations (4) and the Newton equations (5) represent the equations of motion (EOM) of the NA-QMD approach. They are valid in *any* basis for the functions ψ^j. In the current study atomic orbitals represented by Slater type orbitals are used. They guarantee the correct

asymptotic behavior of the density, which is essential for the description of electron transfer processes well-known from ion-atom scattering theory [27]. The exchange-correlation potential V_{xc} is defined within the so-called adiabatic local density approximation [28]. The core electrons are considered to be frozen, because they are energetically far below the valence levels (at least for the alkali atoms considered in this paper).

For further approximations the entire electronic density ρ is split

$$\rho(\mathbf{r},t) = \rho_0(\mathbf{r},\mathbf{R}) + \Delta\rho(\mathbf{r},t). \qquad (6)$$

ρ_0 corresponds to the adiabatic density of the neutral reference system, whereas the explicitly time-dependent term $\Delta\rho$ describes all nonadiabatic and charge effects. By means of the ansatz (6) two simplifying approximations can be introduced [22]. First, the full density ρ in the exchange-correlation terms is replaced by the adiabatic part ρ_0. Second, the Hartree term in the total energy is decomposed with Eq. (6) into three terms with the structures $\rho_0\rho_0$, $\rho_0\Delta\rho$, and $\Delta\rho\Delta\rho$, where the first two are taken fully into account and the last one (which should be small in weakly charged systems) is neglected. This leads to *linear* KS equations which simplifies the numerical solution drastically. The resulting approximate EOM can be written as

$$\dot{a}^j_\alpha(t) = -\sum_{\beta\gamma} (S^{-1})_{\alpha\beta}\left\{ iH^0_{\beta\gamma} + \sum_A^{N_n} \dot{\mathbf{R}}_A \mathbf{R}^A_{\beta\gamma}\right\} a^j_\gamma(t) \qquad (7)$$

and

$$M_A\ddot{\mathbf{R}}_A = -\frac{\partial}{\partial R_A}U(\mathbf{R}) - \sum_j^{N_e}\left\{ \sum_{\alpha\beta} \bar{a}^j_\alpha\left(\frac{\partial H^0_{\alpha\beta}}{\partial R_A}\right)a^j_\beta \right.$$
$$-\sum_{\alpha\beta\gamma\delta}[\bar{a}^j_\alpha H^0_{\alpha\beta}(S^{-1})_{\beta\gamma}\mathbf{R}^A_{\gamma\delta}a^j_\delta$$
$$\left. +\bar{a}^j_\alpha(\mathbf{R}^T)^A_{\alpha\beta}(S^{-1})_{\beta\gamma}H^0_{\gamma\delta}a^j_\delta]\right\} \qquad (8)$$

with the Hamilton matrix

$$H^0_{\alpha\beta} \equiv \langle \phi_\alpha | \hat{t} + V_{\text{eff}}[\rho_0](\mathbf{r},t) | \phi_\beta\rangle, \qquad (9)$$

where the density ρ within the effective potential (2) was replaced by ρ_0 and the external potential is to be understood as a sum of Coulomb and frozen-core potentials. This adiabatic Hamilton matrix $H^0_{\alpha\beta}$ is calculated in a two-center approximation [29] similar to the method described in [30]. The conservative potential $U(\mathbf{R})$ is defined by

$$U(\mathbf{R}) \equiv \frac{1}{2}\sum_A^{N_n} \sum_B^{N_n}{}' \frac{Z^0_A Z^0_B}{|\mathbf{R}_A - \mathbf{R}_B|}$$
$$-\frac{1}{2}\int d^3r \int d^3r' \frac{\rho^0(\mathbf{r},\mathbf{R})\rho^0(\mathbf{r}',\mathbf{R})}{|\mathbf{r}-\mathbf{r}'|}$$
$$-\int d^3r[\rho^0(\mathbf{r},\mathbf{R},t)]^2\frac{\delta\epsilon_{xc}[\rho^0]}{\delta\rho^0(\mathbf{r},\mathbf{R})} \qquad (10)$$

with Z^0_A the valence charge of atom A. Practically, $U(\mathbf{R})$ represents a short-range repulsive potential, because the two large contributions in the first and second line of Eq. (10) cancel each other to a large extent. This is used to approximate $U(\mathbf{R})$ by a sum over pairwise interactions $U(R_{AB})$. These pair potentials are determined using *ab initio* calculations for diatomic molecules [29]. Both, $H^0_{\alpha\beta}$ and $U(R)$, determine the ground-state properties, in particular the geometric structures and ionization potentials, of the clusters (see Sec. III B).

B. Charge transfer probabilities and cross sections

The calculation of CT probabilities in cluster collisions represents a complicated task because many electrons are involved. Rigorous methods based on the time-dependent density are currently not known. A practical way out consists in the construction of many-particle probabilities based on the single-particle KS orbitals. The following considerations are specifically written for cluster–atom collisions, in which the target atom will be well separated from the cluster (or from cluster fragments) before and after the collision.

For the calculation of many-particle probabilities we use a statistical approach similar to a method used for the theoretical study of multiple ionization of clusters [31]. The actual calculation is simplified by the local basis [cf. Eq. (3)] which is also used to represent the stationary KS functions

$$\psi_n(\mathbf{r};\mathbf{R}) = \sum_\beta \phi_\beta(\mathbf{r}-\mathbf{R})C_{\beta n}(\mathbf{R}). \qquad (11)$$

These functions are the solution of the usual stationary KS equations for the actual atomic positions $\mathbf{R}$, where the coefficients $C_{\beta n}$ result from the algebraic equation

$$\sum_\beta (H_{\alpha\beta} - \varepsilon_n S_{\alpha\beta})C_{\beta n} = 0. \qquad (12)$$

In the asymptotic regions $t \to \pm\infty$, where the target atom is well separated, those ψ_n "belonging" to the target can uniquely be assigned.

The probabilities to find the electron described by ψ^j within the stationary state ψ_n can be defined by combining the representations (3) and (11) leading to

$$W^\pm_{jk} = \left| \sum_\beta [C_{\beta k}(\mathbf{R}(t^\pm))]^{-1} a^j_\beta(t^\pm)\right|^2, \qquad (13)$$

where $t^{\pm} = t \to \pm \infty$ (i.e., before and after the collision). With Eq. (13), the transfer probability with respect to the target atom A reads

$$P_j = |W_{jA}^+ - W_{jA}^-|, \quad W_{jA}^{\pm} = \sum_{k \in \{A\}} W_{jk}^{\pm} \qquad (14)$$

with $\{A\}$ the set of indices of all atomic orbitals centered at the target atom A. From these probabilities we calculate *exclusive* many-particle probabilities which are given by the product

$$P(n_1, \ldots, n_J) = \prod_{j=1}^{J} \binom{d_j}{n_j} P_j^{n_j} (1 - P_j)^{d_j - n_j}. \qquad (15)$$

Here, $d_j = 1,2$ is the spin degeneracy, $n_j \leq d_j$ the number of transfered electrons of the KS function ψ^j, and J the number of KS functions. Any combination of the arguments $n_1, \ldots, n_J$ of P corresponds to a certain final charge state q of the target. For specific channels one has to sum up all contributing probabilities (15) to get the probability P_q for the charge state q of the target in one collision as

$$P_q = \sum_{\{n_j\}} P(n_1, \ldots, n_J) \delta_{qs}, \quad s = \sum_{j=1}^{J} n_j (-1)^{1 + W_{jA}^-} \qquad (16)$$

with the Kronecker symbol δ_{qs}, where the sum goes over all possible combinations of the n_j, i.e., all possible electron transfers.

Finally, one has to average the probabilities P_q over all $N_{\text{tot}}(b)$ collision events with impact parameter b

$$\bar{P}_q(b) = \frac{1}{N_{\text{tot}}(b)} \sum P_q. \qquad (17)$$

The statistical uncertainty of this average is estimated by its standard deviation $s_D(b)$. Integrating $\bar{P}_q(b)$ over b yields the integral (or primary) CT cross section

$$\sigma_q = 2\pi \int db \, b \, \bar{P}_q(b). \qquad (18)$$

An error estimation $\Delta\sigma$ for the cross section is obtained as

$$\Delta\sigma = \frac{1}{2}(\sigma^{(\text{hi})} - \sigma^{(\text{lo})}) \qquad (19)$$

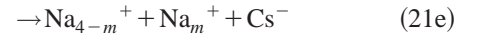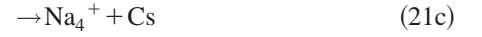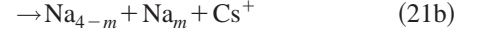using the standard deviation $s_D(b)$ of the probability in

$$\sigma^{(\text{hi,lo})} = 2\pi \int db \, b \, [\bar{P}_q(b) \pm 2s_D(b)]. \qquad (20)$$

III. COLLISIONS OF SODIUM-CLUSTER IONS WITH CAESIUM ATOMS

A. Detailed analysis of tetramer collisions

The complexity of nonadiabatic cluster collisions can already be demonstrated by considering the comparatively

small system $Na_4^+ + Cs$. In the collision energy range of a few keV (in particular at 2.7 keV used in the experiment [3,4]) the following reaction channels have to be considered [20]:

$$Na_4^+ + Cs \to Na_4 + Cs^+ \qquad (21a)$$

$$\to Na_{4-m} + Na_m + Cs^+ \qquad (21b)$$

$$\to Na_4^+ + Cs \qquad (21c)$$

$$\to Na_{4-m}^+ + Na_m + Cs \qquad (21d)$$

$$\to Na_{4-m}^+ + Na_m^+ + Cs^- \qquad (21e)$$

taking into account in channel (21e) that Na_4^{++} is certainly unstable. In the experiment [3,4] the CT cross section was determined by detecting the neutralized nonfragmented clusters, i.e., channel (21a) was measured exclusively. In this setup all other reactions, in particular (21b), have to be considered as competing channels. The fragmentation of the cluster, however, may result from secondary statistical decay processes initiated by collision-induced excitation on time scales, which are for cluster-collision experiments typically in the range of microseconds. This represents a general and tough problem for the comparison of results from microscopic simulations with experimental data influenced by statistical decay processes, because the relevant time scales cannot be covered by any molecular dynamics method. Consequently, the influence of the secondary fragmentation processes has to be estimated based on the results from the simulation of the collision process (covering typically a few up to ~ 100 fs for collision energies in the keV range). A method capable of such an estimation, which has been applied successfully for the determination of the CT cross section corresponding to (21a) in Ref. [20], is described in the following.

For the simulations described in the following the Na_4^+ projectile is prepared in its electronic and geometric ground state (rhombic D_{2h}; see Fig. 5 and related discussion in Sec. III B). Analyzing the simulations of $Na_4^+(2.7 \text{ keV}) + Cs$ collisions event by event a strong dependence of the CT probability P_+ on the initial orientation of the cluster is observed, which is shown in the upper panel of Fig. 1 as a function of the impact parameter b (5300 events). $P_+ \equiv P(Cs^+)$ represents the integral CT probability to find Cs^+ in the exit channel without regard to the evolution of the cluster corresponding to an "integral" over channels (21a) and (21b) (for details of the probability calculations see Sec. II B). The b-weighted integration of the mean probability $\bar{P}_+(b)$ according to Eq. (17) (thick line in the upper panel of Fig. 1) yields with Eq. (18) an integral CT cross section $\sigma_+ = (38 \pm 2)$ Å^2 [20], which is considerably larger than the experimental value $\sigma_{\text{CT}}^{\text{expt}} = (17 \pm 3)$ Å^2 [3] due to the competing fragmentation channel (21b).

A typical fragmentation event observed on the simulated time scale (80 fs) is illustrated in Fig. 2. Due to the collision geometry a nearly binary collision between one sodium atom
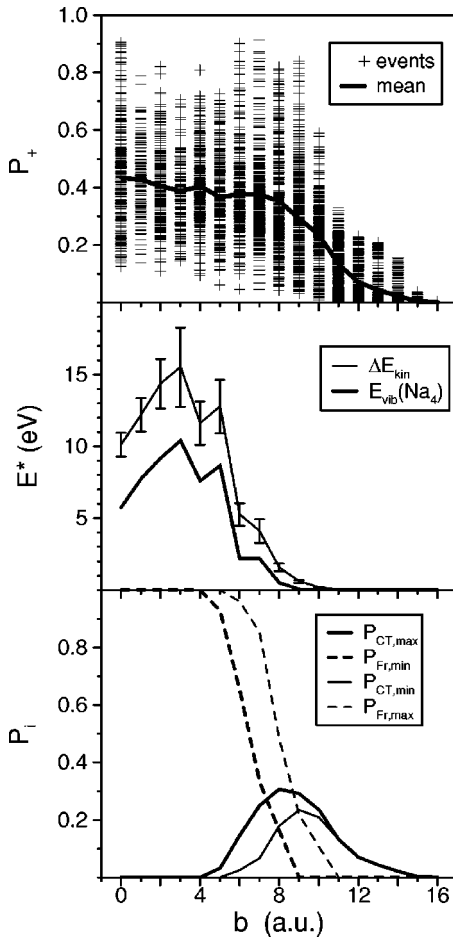
FIG. 1. Calculated integral CT probability P_+ (upper panel) for all simulated events ($+$) and orientation-averaged (thick line), mean kinetic-energy loss ΔE_{kin} and mean vibrational kinetic energy E_{vib} (middle panel) for ''intact'' clusters after the collision (see text), as well as upper and lower limit for the exclusive CT probability $P_{\mathrm{CT,max}}$ and $P_{\mathrm{CT,min}}$, respectively, obtained along with the limiting fragmentation probabilities $P_{\mathrm{Fr,min}}$ and $P_{\mathrm{Fr,max}}$ (lower panel; see text) as functions of the impact parameter b for $Na_4^+(2.7$ keV$)$ $+$Cs collisions. The length of the error bars is given by $2\,s_{\mathrm{D}}$, where s_{D} is the standard deviation of the orientation average.

and the caesium atom occurs resulting in a momentum transfer to this sodium atom sufficient for direct fragmentation (''impulsive fragmentation'' [23,21]). Such direct fragmentation events are rather likely (14% of all events) especially for small impact parameters ($b \lesssim 5$ a.u.). The second fragmentation mechanism, which is important also for larger impact parameters ($b \lesssim 10$ a.u.), is illustrated in Fig. 3. In the shown event, the cluster exhibits (almost) no excitation in the nuclear degrees of freedom (i.e., no vibration; see upper row in Fig. 3). However, a considerable amount of electronic excitation energy has been stored in the cluster (~ 2 eV in this case), which can be transferred into nuclear (vibrational) degrees of freedom via the electron-vibration coupling [21]. Indeed, vibrations begin to develop in the cluster (about 100 fs after the collision; middle row in Fig. 3). Finally (after 2 ps; lower row in Fig. 3), the cluster dissociates into two dimers showing that the transferred vibrational energy ex-
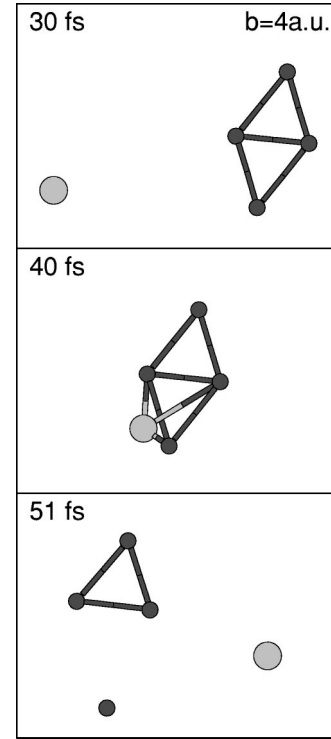

FIG. 2. Snapshots from the time evolution of a typical event for direct or ''impulsive'' fragmentation in $Na_4^+(2.7$ keV$)+$Cs collisions taken before (30 fs after the start of the simulation), during (40 fs) and after the impact (51 fs).

ceeded the dissociation limit. This mechanism has been called ''electronic fragmentation'' [23,21]. Both basically different fragmentation processes have been verified and distinguished experimentally [23].

Depending on the actual excitation energy (and on the number of vibrational degrees of freedom) the cluster may survive in a vibrationally excited state or may undergo statistical fragmentation on a larger time scale. The decay constants can be estimated applying statistical models like RRK or RRKM (see Ref. [32] for an application to sodium clusters). Within these models it can easily be seen that on the experimental time scale (μs) already a small excess energy (i.e., the energy above the dissociation limit) leads to a vanishing ''survival probability'' for a vibrationally excited cluster. E.g., the simple RRK expression for the decay time τ as a function of the vibrational excitation energy E_{vib}^* reads [32]

$$\tau(E_{\mathrm{vib}}^*) = \nu^{-1}\left(1 - \frac{D_n}{E_{\mathrm{vib}}^*}\right)^{1-s}, \tag{22}$$

where ν, D_n, and $s = 3n - 6$ stand for the (mean) mode frequency, the dissociation limit for cluster size n, and the number of vibrational degrees of freedom, respectively. Inserting the bulk phonon frequency $\nu = 3.1 \times 10^{12}$ s^{-1}, $s = 6$ for Na_4, and $D_4 = 0.44$ eV obtained for the favored decay channel $Na_4 \rightarrow Na_2 + Na_2$ with the NA-QMD approach, and an excitation energy $E_{\mathrm{vib}}^* = 0.49$ eV one obtains $\tau = 29$ ns, which is (at least) two orders of magnitude smaller than the experi-
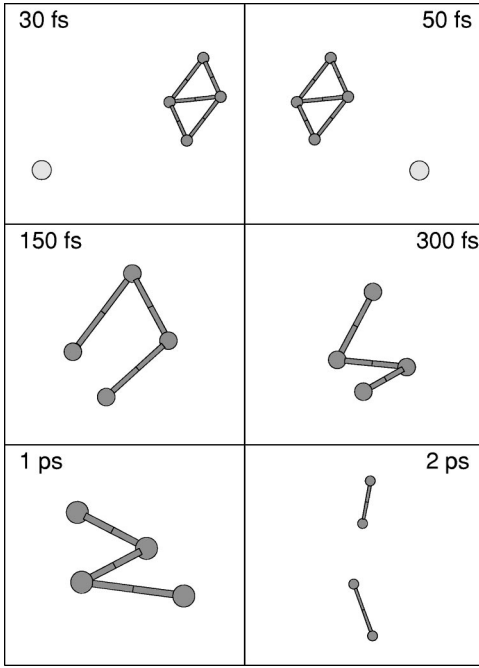
FIG. 3. Snapshots from the time evolution of a typical event for ''electronic'' fragmentation in Na_4^+(2.7 keV)+Cs collisions (b =8 a.u.): cluster and atom are passing each other (upper row), electronic excitation in the cluster is transferred into vibrational excitation (middle row) leading finally to the dissociation into two dimers (after 2 ps).

mental time scale. Because of the exponential decay law $\exp[-t/\tau]$ it becomes obvious that practically all excited clusters will decay if the vibrational excitation energy exceeds the dissociation limit.

In the middle part of Fig. 1 the mean value of the kinetic energy loss in the relative motion ΔE_{kin} and of the actual kinetic energy of the vibrations E_{vib} calculated at the end of the simulation ($t=80$ fs) are shown as a function of the impact parameter b, where the average was taken over all those events, in which the cluster has not yet fragmented. ΔE_{kin} represents in a given event the total excitation energy in the system, i.e., the reservoir of energy available for secondary processes. The shown mean values indicate that for $b\leqslant5$ a.u. almost all clusters would certainly decay in a continued simulation. Up to $b=10$ a.u. enough energy can be available for fragmentation. However, at least a part of the excitation energy is stored as electronic excitation dominating in the range $5\leqslant b\leqslant10$ a.u. The amount of electronic energy, which will actually be transferred into vibrational energy, can hardly be estimated without further calculation. (Note that even for Na_4 NA-QMD simulations on a time scale of 1 ps would be unaffordably expensive if the same level of event statistics as shown in the upper panel of Fig. 1 should be reached.)

The single values of ΔE_{kin} for every event are used to obtain an *upper limit* for the fragmentation probability $P_{Fr,max}(b)$ by counting all those events as fragmentation events, in which this total excitation energy is larger than the (theoretical value of the) dissociation limit $D_4=0.44$ eV. This corresponds to the extreme case, where the whole exci-

tation energy is transferred into vibrational degrees of freedom. On the other hand, if the actual value of the kinetic energy of the vibrations E_{vib} is at the end of the simulation already larger than D_4 this event will certainly exhibit fragmentation on a larger time scale (see discussion above). Because only the kinetic part of the vibrational excitation energy is taken into account, one obtains a *lower limit* for the fragmentation probability $P_{Fr,min}(b)$ by counting the events with $E_{vib}>D_4$ as fragmentation events. The fragmentation probability is estimated by the relative abundance $P_{Fr}(b)$ $\approx N_{Fr}(b)/N_{tot}(b)$ with N_{Fr} and N_{tot} the number of fragmentation events and the total number of simulated events, respectively, at a given impact parameter b. The fragmentation cross section can be calculated from P_{Fr} analogue to Eq. (18). The resulting probabilities $P_{Fr,max}$ and $P_{Fr,min}$ along with the corresponding $P_{CT,min}$ and $P_{CT,max}$ for channel (21a) were drawn in the lower panel of Fig. 1. The ''real'' probabilities have to be inbetween the limiting cases, which are estimated simply by the average of the maximum and the minimum probability $P_i=(P_{i,max}+P_{i,min})/2$ with $i=$ ''Fr'' for the total fragmentation probability, i.e., channels (21b) +(21d), and $i=$ ''CT'' for the CT probability, i.e., channel (21a). Note that the limiting cross sections corresponding to $P_{Fr,max}$ and $P_{Fr,min}$ differ only by a factor of 1.5 in this case (1.4 for CT). These averaged probabilities will be used in the following to calculate exclusive CT and fragmentation cross sections.

With the procedure described above a CT cross section $\sigma_{CT}=20$ Å^2 was obtained [20], which is still slightly larger than the experimental value. The calculations presented so far have been carried out with zero initial temperature in the cluster. Laser ionization of neutral sodium clusters as used in the experiment [3,4] to produce the projectile ions, however, is accompanied by a considerable ''heating'' of the cluster. Although the actual temperature cannot be measured directly, it could be demonstrated in other experiments [33] that laser ionization leads to ''liquid'' sodium cluster ions. The term ''liquid'' means that the constituent atoms can move throughout the cluster volume (or within the accessible phase space) without a definite topology.

In order to investigate the influence of an initial cluster temperature, long-time simulations (300 ps) of vibrationally excited clusters have been performed with different excitation energies covering the range up to the dissociation limit. The excitation energy has been controlled by distorting the rhombus ground-state geometry, which guarantees zero total linear and angular momentum of the cluster. From these trajectories snapshots were stored on a coarse time grid to serve as initial configurations for the simulation of the collisions. The orientation average used in the calculations at zero initial temperature is replaced by an average over randomly selected configurations from the time evolution of vibrationally excited clusters with a given excitation energy. (Note that on the time scale of the collision with 2.7 keV incident energy the thermal motion appears to be frozen.)

The obtained CT and fragmentation cross sections are shown in Fig. 4 as a function of the initial cluster temperature T, where the simple correspondence $E_{vib}^*=(3n-6)kT$ has been used to ''translate'' the vibrational energy into a
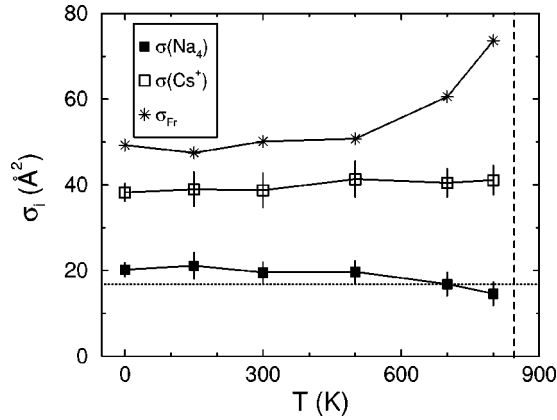
FIG. 4. Calculated exclusive and integral CT cross section [$\sigma_{CT} \equiv \sigma(Na_4)$ and $\sigma_+ \equiv \sigma(Cs^+)$, respectively] as well as the total fragmentation cross section σ_{Fr} as functions of the initial cluster temperature T for Na_4^+ (2.7 keV) + Cs collisions.

temperature scale. The integral CT cross section $\sigma_+ \equiv \sigma(Cs^+)$, i.e., for channels (21a)+(21b), exhibits a very weak dependence on the temperature slightly enhanced in the range of ''liquid'' clusters ($T \geq 500$ K), whereas the fragmentation cross section σ_{Fr} increases considerably in this temperature range, because less collision-induced excitation is needed for fragmentation. Consequently, the exclusive CT cross section $\sigma_{CT} \equiv \sigma(Na_4)$ for channel (21a) decreases with increasing temperature. At $T = 700$ K, i.e., about 0.1 eV below the dissociation limit $T(D_4) \approx 850$ K (indicated by the dashed vertical line in Fig. 4), the CT cross section $\sigma_{CT} = 16.8$ Å^2 agrees perfectly with the experimental value (indicated by the dotted horizontal line in Fig. 4). This ''energetic distance'' of 0.1 eV below the dissociation limit has been used [20] as an estimation of the initial cluster temperature in the experiment [3,4] and is applied for the other considered cluster sizes as well, which are investigated in the following section.

B. Structure dependence of the cross sections

In order to illustrate the variety of geometric structures of sodium-cluster cations, the three most stable isomers obtained in the NA-QMD approach are shown in Fig. 5. (The geometric structures have been determined for the electronic ground state.) Most of these isomers were also found in *ab initio* structure calculations [34–36]. Comparing qualitatively, the same ground state is obtained for $n = 4,6,7,11$ as in CI calculations [36], and for $n = 8,9$ only the isomer sequence in energy differs. The only serious discrepancy concerns the pentamer, because the planar trapezoidal structure (second row, left column in Fig. 5) was not found to be a stable minimum on the *ab initio* level [34–36].

The reproduction of (approximately) the correct ionization potentials represents an essential precondition for the calculation of *absolute* CT cross sections. The calculated vertical ionization potentials I_P of the (neutral) clusters agree remarkably well with the experimental data [37] as shown in Fig. 6. The calculated ionization potential of the Cs atom fits the experimental value of 3.9 eV.
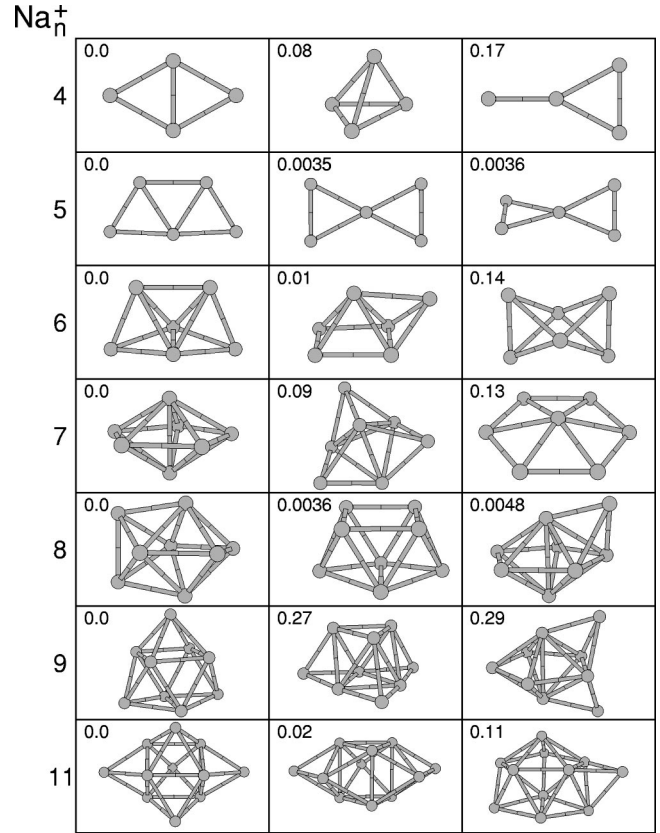
Na_n^+

FIG. 5. Ground-state structures (left column) and first two isomers (middle and right column) of sodium cluster ions obtained within the NA-QMD approach for the considered cluster sizes. The numbers in the boxes indicate the energetic differences (in eV) with respect to the structure lowest in energy.

For all structures shown in Fig. 5 the CT cross section σ_{CT} corresponding to the analogue of channel (21a), i.e.,

$$Na_n^+ (2.7 \text{ keV}) + Cs \rightarrow Na_n + Cs^+, \qquad (23)$$
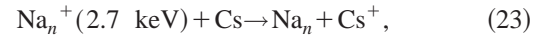
has been calculated and plotted in the upper panel of Fig. 7 as a function of the cluster size n in comparison with the
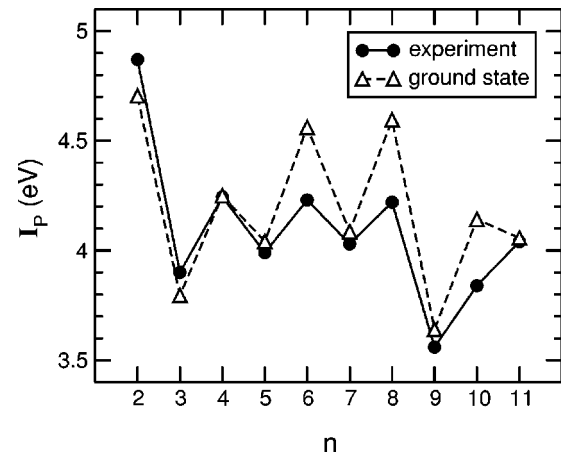

FIG. 6. Calculated vertical ionization potentials I_P for the structures lowest in energy (cf. left column in Fig. 5) as a function of the cluster size n in comparison with experimental data [37].
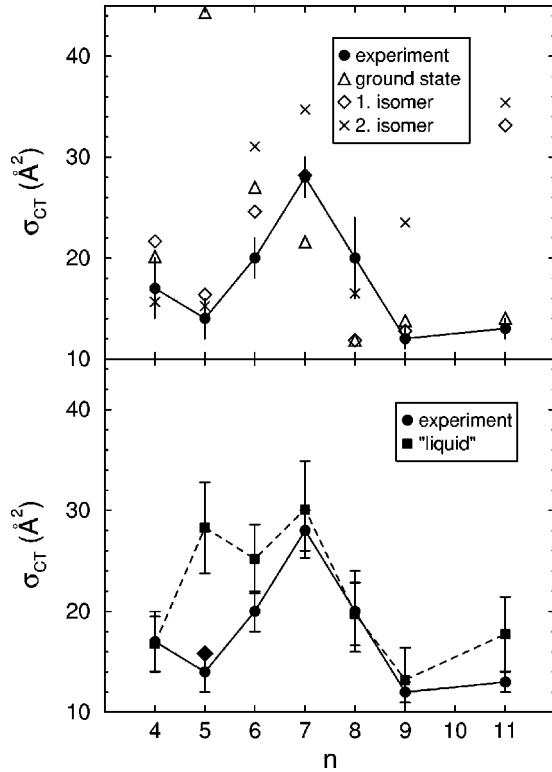
FIG. 7. Calculated exclusive CT cross sections σ_{CT} in Na_n^+(2.7 keV)$+$Cs collisions with zero initial temperature in the cluster (upper panel) for all structures shown in Fig. 5 and for ''liquid'' cluster ions (lower panel) compared with the experimental data [3].

FIG. 8. Calculated total fragmentation cross sections σ_{Fr} in Na_n^+(2.7 keV)$+$Cs collisions with zero initial temperature in the cluster for the ground state isomers shown in Fig. 5 as well as for ''liquid'' clusters as functions of the cluster size n compared with two geometrical models (see text).

measured data [3] (not available for $n=10$). Large variations for different isomers at a given cluster size are found, which can be made plausible by considering the electronic single-particle levels in the stationary KS basis (cf. Sec. II B). An inspection of the corresponding occupation numbers indicates that the (valence) electron of the Cs atom is transferred preferably into an initially unoccupied orbital of the cluster in the energetic vicinity of the Cs($6s$) level. These (comparatively high-lying) cluster levels reflect structural changes distinctly and, thus, vary the character of the CT process inbetween off-resonant and quasiresonant resulting in the large differences found for σ_{CT} (cf., e.g., $n=11$ in the upper panel of Fig. 7). With the theoretical cross sections for the ground-state structures (cf. left column in Fig. 5), i.e., assuming zero temperature in the projectile clusters, the variation of the experimental CT cross sections with the cluster size cannot be reproduced.

Calculations with ''liquid'' cluster ions in the initial state have been performed applying the same procedure and the same temperature estimation as discussed for the tetramer case (see previous section), i.e., the initial excitation energy was chosen (approximately) 0.1 eV below the size-dependent dissociation limit. The resulting CT cross sections σ_{CT} are compared with the measured data in the lower panel of Fig. 7. Except the case $n=5$, which is discussed below, the theoretical cross sections calculated on an *absolute* scale [20] are in agreement with the experimental data. In particular, the maximum of the experimental CT cross section at
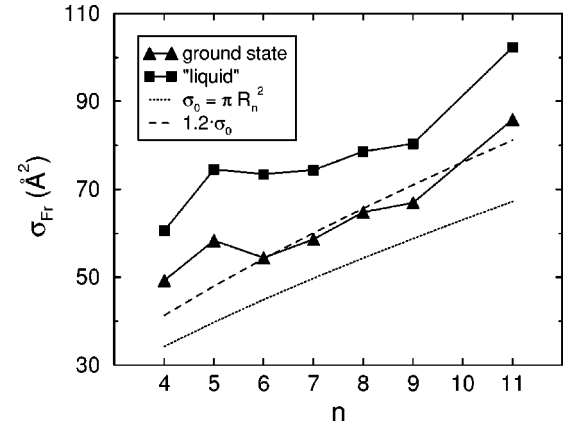
$n=7$ is reproduced by the calculations. That this is not peculiar to the particular collision energy (2.7 keV) was demonstrated by investigating the collision-energy dependence of the CT cross sections [20]. The statistical error bars of the calculated cross sections result from a conservative error estimation (see Sec. II B) and reflect the large variations of the outcome of the collision with the initial configuration as illustrated in the upper panel of Fig. 1. A considerable reduction of these uncertainties (especially for $n\geq 7$) would require unaffordably high computational costs.

For the trapezoidal structure of the pentamer, which represents the energetically favored structure in the NA-QMD approach but found to be unstable in *ab initio* structure calculations (see discussion above), a comparatively large CT cross section (≈ 45 Å^2; cf. upper panel of Fig. 7) was obtained as a consequence of the particular electronic structure providing quasiresonant conditions for the CT with the Cs atom. In the simulations with ''liquid'' cluster ions this structure and related similar structures contribute to the average over randomly chosen configurations (see previous section) leading to a larger CT cross section compared to the measured value. This can be demonstrated by taking a simple average over the cross sections for the first and second isomer (indicated by the diamond in the lower panel of Fig. 7), which agrees within the statistical errors with the experimental value.

The dependence of the total fragmentation cross section on the cluster size is shown in Fig. 8. The calculated cross sections for the ground-state structures (assuming $T=0$) are considerably larger than the geometrical cross section $\sigma_0 = \pi R_n^2$ corresponding to the ''jellium'' model radius $R_n = r_s n^{1/3}$ with the bulk Wigner-Seitz radius $r_s = 3.93$ a.u. (dotted line in Fig. 8). This is interpreted as the result of an effective ''electronic fragmentation'' (discussed in the previous section), because the ''electronic cloud'' occupies a larger volume compared to the structure of the nuclei. The general trend can be reasonably described by scaling the geometrical cross section with a factor of 1.2 ($1.2\sigma_0$; dashed line in Fig. 8). The deviations from this ''average'' are con-

sidered as particular structure effects. The enhanced cross sections for $n \lesssim 5$ indicate the transition from planar to non-planar structures going from $n = 5$ to $n = 6$ (cf. Fig. 5). The slightly smaller calculated cross section at $n = 9$ result from the particular stability of the electronic ''closed shell'' structure (8 valence electrons). The ground-state structure of Na_{11}^+ (first column, last row in Fig. 5) exhibits a conspicuous prolate shape leading to a somewhat enhanced cross section. The fragmentation cross sections are considerably larger in collisions with ''liquid'' cluster ions due to the initial vibrational energy in the system. The size dependence follows about the same trend as for the ground-state structures corresponding to the increasing geometrical cross section with increasing cluster size.

The calculated fragmentation cross sections plotted in Fig. 8 include all relevant processes: direct or ''impulsive'' fragmentation (cf. Fig. 2), ''electronic fragmentation'' (cf. Fig. 3), and (approximately) also secondary statistical decay processes. Although the measurement of absolute fragmentation cross sections represents a very difficult experimental task, such data (not available at present) could help to check not only the discussed results, but also, more generally, the validity of the theoretical concepts behind, in particular the procedure to take into account statistical decay processes (cf. Sec. III A).

C. An exotic channel: Anion formation

An experimental setup detecting the formed target ions Cs^q after the collision with cluster ions could provide integral CT cross sections, i.e., without regard to the evolution of the cluster. In Ref. [20] a finite probability for the formation of anions Cs^- in Na_4^+ (2.7 keV) + Cs collisions was predicted—an ''exotic'' channel, because it represents the inverse of the ''normal'' CT process (23). The calculated integral CT cross sections $\sigma_+ \equiv \sigma(Cs^+)$ and $\sigma_- \equiv \sigma(Cs^-)$ in Na_n^+(2.7 keV) + Cs are shown as a function of the cluster size n in Fig. 9. Obviously, the cross sections for the ''normal'' CT process with Cs^+ in the exit channel are considerably larger (at least a factor of two) than for the anion formation, and the size dependences show up completely different.

The size dependence of σ_+ exhibits a strong similarity to that of the exclusive CT cross section $\sigma_{CT} \equiv \sigma(Na_n)$ for channel (23), which holds for $T = 0$ as well as for ''liquid'' projectile clusters. The absolute values of σ_+, however, are considerably larger than those of σ_{CT}, because the fragmentation channels deplete the integral CT cross section ($\sigma_+ > \sigma_{CT}$). In the special case $n = 8$ this depletion is less pronounced because of the particular stability of *neutral* Na_8, which is indicated (for ''liquid'' clusters) by switching $\sigma_+(n = 8) \lesssim \sigma_+(n = 9)$ (cf. Fig. 9) into $\sigma_{CT}(n = 8) > \sigma_{CT}(n = 9)$ (cf. Fig. 7).

In the size dependence of σ_- a conspicuous odd-even alternation (for $n \lesssim 9$) with enhanced cross sections for odd numbers of valence electrons in the projectile ion can be observed (lower region of Fig. 9). Surprisingly, a weak (partly negligible) temperature dependence is found for σ_- in contrast to the findings for σ_+ (and σ_{CT}). Both observa-
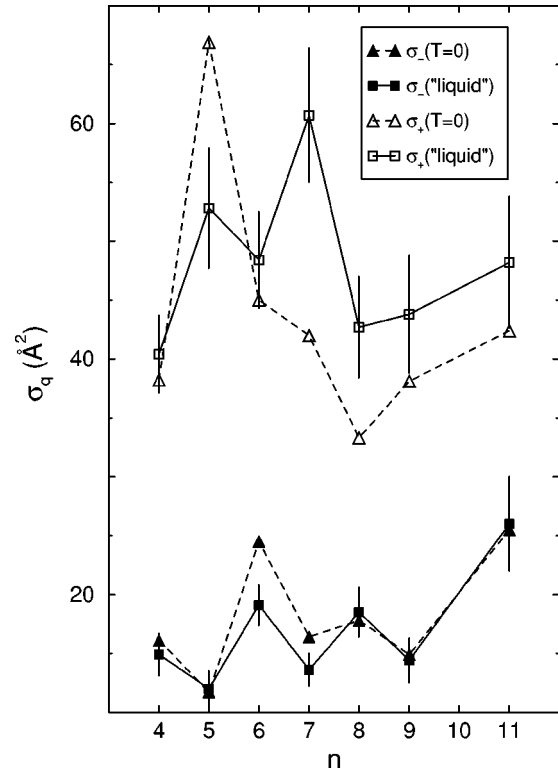

FIG. 9. Calculated integral cross sections for the formation of Cs anions σ_- and cations σ_+ in Na_n^+(2.7 keV) + Cs collisions with zero initial temperature in the cluster for the ground state isomers shown in Fig. 5 as well as for ''liquid'' clusters as functions of the cluster size n.

tions can be explained qualitatively by considering the electronic single-particle levels in the stationary KS basis (cf. Sec. II B). For an odd number of valence electrons in the cluster ion (i.e., even n) the highest occupied KS orbital is energetically closer to the $Cs(6s)$ level compared to a situation with an even number of electrons. This provides more favorable conditions for the transfer of an electron from the cluster ion to the Cs atom in the case of even n. This argument is, of course, only appropriate in the small size range $4 \lesssim n \lesssim 9$. Already at $n = 11$ (belonging to the next ''electronic shell'' in a shell model picture) the highest occupied orbital is again quite close to the Cs level resulting in a relatively large cross section σ_-. The weak temperature dependence of σ_- results from the ''robustness'' of the initially occupied, low-lying levels in the cluster (where the electron producing Cs^- has to come from) against structural changes, whereas the orbitals involved in the ''normal'' CT process yielding Cs^+ reflect structural changes more distinctly (cf. related discussion in the previous section).

Cs anions have been the subject of investigation in atomic physics (for a review see [38]) as well as in chemistry, where they have been found to exist in solution and in the solid state (e.g., as so-called alkalides Cs^+(complexant) $\times Cs^-$ [39]). The ground state of Cs^- ($6s^2\,^1S$) is expected to be bound [40,38]. Moreover, the stability issue of excited states is under current investigation [41]. Thus, our prediction of anion formation in cluster–atom collisions leaves room for

further investigations, especially if an experimental verification could be achieved in the future.

IV. SUMMARY

The complexity of nonadiabatic cluster collisions has been illustrated by a detailed analysis of $Na_n^+(2.7\ keV)$ + Cs collisions. Thereby, the interplay between CT and fragmentation or, more generally, the essential couplings between nuclear and electronic degrees of freedom have been investigated with special emphasis on methodical aspects. After the theoretical part describing the NA-QMD approach (Sec. II A) and the statistical method used for the calculation of CT probabilities (Sec. II B) tetramer collisions have been studied in detail (Sec. III A) considering all relevant reaction channels. For the determination of exclusive CT cross sections (i.e., corresponding to a particular channel) all fragmentation processes have to be taken into account. The three different mechanisms—direct or ''impulsive'' fragmentation, ''electronic'' fragmentation and statistical decay—have been discussed. It was shown how the abundance of statistical decay processes can be estimated based on calculated excitation energies after the collision.

For a quantitative comparison with experimental cross sections the initial cluster temperature has to be taken into account, in particular if the clusters are expected to be in a liquid state. In order to obtain a proper description of CT probabilities in collisions with liquid clusters the orientation average used for zero-temperature clusters is replaced by an average over randomly selected configurations from the time evolution of vibrationally excited clusters.

The considerable variance of the CT cross section found for different isomers as well as for different cluster sizes have been attributed to the resonance character of the CT process (Sec. III B) ranging from off-resonant to quasi-resonant conditions. The experimental CT cross sections for $Na_n^+(2.7\ keV)$ + Cs collisions [3] are reproduced on an absolute scale by the calculations assuming ''liquid'' cluster ions in the projectile beam. The size dependence of the predicted total fragmentation cross section follows the trend of a droplet or ''jellium'' model ($n^{2/3}$) with overlaid structure effects.

Our recent prediction of anion formation in cluster-atom collisions [20] has been elaborated in more detail (Sec. III C) predicting integral cross sections for this exotic process. The size dependence of this cross section (odd-even alternation) shows entirely different from that of the ''normal'' CT process, which has been explained considering the behavior of electronic states against structural changes. An experimental verification of this anion formation in cluster collisions, which will hopefully be available in the near future, could open an interesting new field of investigation.

ACKNOWLEDGMENTS

[1] B.H. Bransden and M.R.C. McDowell, *Charge Exchange and the Theory of Ion-Atom Collisions* (Clarendon Press, Oxford, 1992).

[2] For a review including ion-molecule and ion-surface collisions see, e.g., M. Kimura and N.F. Lane, Adv. At., Mol., Opt. Phys. **26**, 79 (1990).

[3] C. Bréchignac, Ph. Cahuzac, J. Leygnier, R. Pflaum, and J. Weiner, Phys. Rev. Lett. **61**, 314 (1988).

[4] C. Bréchignac, Ph. Cahuzac, F. Carlier, J. Leygnier, and I.V. Hertel, Z. Phys. D: At., Mol. Clusters **17**, 61 (1990).

[5] N.D. Bhaskar, R.P. Frueholz, C.M. Klimcak, and R.A. Cook, Chem. Phys. Lett. **154**, 175 (1989).

[6] M. Abshagen, J. Kowalski, M. Meyberg, G. zu Putlitz, J. Slaby, and F. Träger, Chem. Phys. Lett. **174**, 455 (1990).

[7] J.J. Stry and J.F. Garvey, Int. J. Mass Spectrom. Ion Processes **138**, 241 (1994).

[8] B. Farizon, M. Farizon, M.J. Gaillard, E. Gerlic, and S. Ouaskit, Int. J. Mass Spectrom. Ion Processes **144**, 79 (1995).

[9] H. Shen, P. Hvelplund, D. Mathur, A. Bárány, H. Cederquist, N. Selberg, and D.C. Lorents, Phys. Rev. A **52**, 3847 (1995).

[10] S. Pollack, D. Cameron, M. Rokni, W. Hill, and J.H. Parks, Chem. Phys. Lett. **256**, 101 (1996).

[11] F. Rohmund and E.E.B. Campbell, Chem. Phys. Lett. **245**, 237

(1995); , Z. Phys. D: At., Mol. Clusters **40**, 399 (1997).

[12] B. Walch, C.L. Cocke, R. Völpel, and E. Salzborn, Phys. Rev. Lett. **72**, 1439 (1994).

[13] T. LeBrun, H.G. Berry, S. Cheng, R.W. Dunford, H. Esbensen, D.S. Gemmel, E.P. Kanter, and W. Bauer, Nucl. Instrum. Methods Phys. Res. B **98**, 479 (1995).

[14] F. Chandezon, C. Guet, B.A. Huber, D. Jalabert, M. Maurel, E. Monnand, C. Ristori, and J.C. Rocco, Nucl. Instrum. Methods Phys. Res. B. **98**, 482 (1995).

[15] Z. Roller-Lutz, Y. Wang, H.O. Lutz, U. Saalmann, and R. Schmidt, Phys. Rev. A **59**, R2555 (1999).

[16] U. Thumm, J. Phys. B **28**, 91 (1995).

[17] N. Selberg, A. Bárány, C. Biedermann, C.J. Setterlind, H. Cederquist, A. Langereis, M.O. Larrson, A. Wänneström, and P. Hvelplund, Phys. Rev. A **53**, 874 (1996).

[18] M. Guissani and V. Sidis, Z. Phys. D: At., Mol. Clusters **40**, 221 (1997).

[19] K.J. Børve and J.P. Hansen, Z. Phys. D: At., Mol. Clusters **25**, 247 (1993).

[20] O. Knospe, J. Jellinek, U. Saalmann, and R. Schmidt, Eur. Phys. J. D **5**, 1 (1999).

[21] U. Saalmann and R. Schmidt, Phys. Rev. Lett. **80**, 3213 (1998).

[22] U. Saalmann and R. Schmidt, Z. Phys. D: At., Mol. Clusters **38**, 153 (1996).

[23] J.A. Fayeton, M. Barat, J.C. Brenot, H. Dunet, Y.J. Picard, U. Saalmann, and R. Schmidt, Phys. Rev. A **57**, 1058 (1998).

[24] T. Schlathölter, O. Hadjar, R. Hoekstra, and R. Morgenstern, Phys. Rev. Lett. **82**, 73 (1999).

[25] E. Runge and E.K.U. Gross, Phys. Rev. Lett. **52**, 997 (1984).

[26] E.K.U. Gross, J.F. Dobson, and M. Petersilka, in *Density Functional Theory*, edited by R. F. Nalewajski, Springer Topics in Current Chemistry Vol. 181 (Springer, Berlin, 1996), p. 81.

[27] D.A. Micha and K. Runge, in *Time-dependent Quantum Molecular Dynamics*, edited by J. Broeckhove and L. Lathouwers (Plenum Press, New York, 1992), p. 247.

[28] E.K.U. Gross and W. Kohn, Adv. Quantum Chem. **21**, 255 (1990).

[29] U. Saalmann, Ph.D. thesis, Dresden, 1996 (unpublished).

[30] D. Porezag, T. Frauenheim, T. Köhler, G. Seifert, and R. Kaschner, Phys. Rev. B **51**, 12 947 (1995).

[31] C.A. Ullrich, P.-G. Reinhard, and E. Suraud, J. Phys. B **30**, 5043 (1997).

[32] C. Brechignac, Ph. Cahuzac, J. Leygnier, and J. Weiner, J. Chem. Phys. **90**, 1492 (1989).

[33] Th. Reiners, W. Orlik, Ch. Ellert, M. Schmidt, and H. Haber-

land, Chem. Phys. Lett. **215**, 357 (1993); Ch. Ellert, M. Schmidt, Ch. Schmitt, Th. Reiners, and H. Haberland, Phys. Rev. Lett. **75**, 1731 (1995).

[34] J.L. Martins, J. Buttet, and R. Car, Phys. Rev. B **31**, 1804 (1985).

[35] V. Bonačić-Koutecký, I. Boustani, M. Guest, and J. Koutecký, J. Chem. Phys. **89**, 4861 (1988).

[36] V. Bonačić-Koutecký, J. Pittner, C. Fuchs, P. Fantucci, M.F. Guest, and J. Koutecký, J. Chem. Phys. **104**, 1427 (1996).

[37] M.M. Kappes, M. Schär, U. Röthlisberger, C. Yeretzian, and E. Schumacher, Chem. Phys. Lett. **143**, 251 (1988).

[38] S.J. Buckman and C.W. Clark, Rev. Mod. Phys. **66**, 539 (1994).

[39] R.H. Huang, D.L. Ward, M.E. Kuchenmeister, and J.L. Dye, J. Am. Chem. Soc. **109**, 5561 (1987); J.L. Dye and M.G. De-Backer, Annu. Rev. Phys. Chem. **38**, 271 (1987).

[40] J. Slater, F.H. Read, S.E. Novick, and W.C. Lineberger, Phys. Rev. A **17**, 201 (1978).

[41] M. Scheer, J. Thøgersen, R.C. Bilodeau, C.A. Brodie, H.K. Haugen, H.H. Andersen, P. Kristensen, and T. Andersen, Phys. Rev. Lett. **80**, 684 (1998).